A Model of Na^+/H^+ Exchanger and Its Central Role in Regulation of pH and Na^+ in Cardiac Myocytes

Chae Young Cha,[†‡] Chiaki Oka,[‡] Yung E. Earm,[§] Shigeo Wakabayashi,[¶] and Akinori Noma[†*]

[†]Biosimulation Project, Faculty of Bioinformatics, Ritsumeikan University, Kusatsu, Japan; [‡]Biosimulation Project, Graduate School of Medicine, Kyoto University, Kyoto, Japan; [§]Department of Physiology, Seoul National University, Seoul, Korea; and [¶]Department of Molecular Physiology, National Cardiovascular Center Research Institute, Osaka, Japan

ABSTRACT A new kinetic model of the Na^+/H^+ exchanger (NHE) was developed by fitting a variety of major experimental findings, such as ion-dependencies, forward/reverse mode, and the turnover rate. The role of NHE in ion homeostasis was examined by implementing the NHE model in a minimum cell model including intracellular pH buffer, Na^+/K^+ pump, background H^+, and Na^+ fluxes. This minimum cell model was validated by reconstructing recovery of pH_i from acidification, accompanying transient increase in $[Na^+]_i$ due to NHE activity. Based on this cell model, steady-state relationships among pH_i, $[Na^+]_I$, and $[Ca^{2+}]_i$ were quantitatively determined, and thereby the critical level of acidosis for cell survival was predicted. The acidification reported during partial blockade of the Na^+/K^+ pump was not attributed to a dissipation of the Na^+ gradient across the membrane, but to an increase in indirect H^+ production. This NHE model, though not adapted to the dimeric behavioral aspects of NHE, can provide a strong clue to quantitative prediction of degree of acidification and accompanying disturbance of ion homeostasis under various pathophysiological conditions.

INTRODUCTION

Several types of pH-related transporters are present in the sarcolemma of cardiac myocytes. Among them, the Na^+-H^+ exchanger (NHE) is regarded as the main acid extruder, in that its H^+ flux is much larger than that of the other acid extruder, the Na^+-HCO_3^- cotransporter (1,2). In addition, abnormal enhancement of NHE activity under acidosis potentially induces intracellular Na^+ overload through Na^+ influx during pumping out excess H^+ (3) and eventually Ca^{2+} overload by depressing the Na^+-Ca^{2+} exchanger (NCX). For example, the enhanced NHE has been reported to play a critical role in ischemia/reperfusion injury (4,5), and slow force response (6,7). Since regulation of all intracellular H^+, Na^+, and Ca^{2+} concentrations within a physiological range is of vital importance in maintaining the excitability, contractility, and cell volume regulation in cardiac myocytes, a dynamic NHE model is indispensable to investigate mechanisms underlying the cellular ionic homeostasis as well as its failure under pathophysiological conditions using mathematical cell models.

A variety of mathematical models of NHE has been developed. Leem et al. (1) derived an empirical polynomial equation based on their measurements of pH_i-NHE flux relationships, and this model was used for exploring effects of acidosis on contraction and membrane excitation (8,9). NHE activity has also been described with Hill equations (10) or by a simple kinetic model (11) that attributed NHE activation to binding of intracellular H^+ to its modifier site. These simple models were easy to apply, but did not provide any details of the dependencies on the intra- and extracellular concentrations of H^+ and Na^+, except for pH_i. Recently, more-complicated kinetic NHE models have been proposed (12–15), but even the latest NHE model (14) did not take account of extracellular H^+ or Na^+ dependencies. In addition to these classical NHE schemes, model development based on the dimer configuration of NHE (16) has been attempted (17–20). However, these models are quite different from each other and it is still difficult to distinguish them experimentally. Furthermore, in cardiac myocytes no positive proof is demonstrated for the cooperative operation of monomers within the dimeric composition. Thus, there is no available NHE model with sufficient detail to predict the contribution of NHE in intact myocytes.

In this study, we developed an NHE model, which satisfactorily reconstructs the dependencies on the intra- and extracellular concentrations of H^+ and Na^+ reported in the systematic experiments in the Purkinje fiber (21,22), in addition to the experimental findings in the transfected cell line (15). Subsequently, we implemented the new NHE model in a simple cell model, and found that original recordings of pH_i and $[Na^+]_i$ variations in experiments were well explained by the alteration of NHE activity. We then examined the role of NHE under pathophysiological conditions by considering the steady-state relationship between pH_i and $[Na^+]_i$ during depression of active Na^+ transport or during long-lasting acidosis.

METHODS

Development of the NHE model scheme

A variety of kinetic schemes, such as ping-pong (12,13), simultaneous ion-transporting (17,18), or dimer models (19,20) have been suggested for NHE. These model schemes might equally well explain experimental findings.

Submitted November 5, 2008, and accepted for publication August 21, 2009.

*Correspondence: noma@sk.ritsumei.ac.jp

Editor: Michael Pusch.

0006-3495/09/11/2674/10 $2.00

doi: 10.1016/j.bpj.2009.08.053

Because of its applicability to a wide range of experimental data, we adopted a ping-pong scheme with 1:1 stoichiometry. Consideration of the dimeric model schemes is presented in the Supporting Material.

The new kinetic NHE model is composed of two distinct functional units: an ion-exchanging part (j_{exch}) and a proton-modifier part (*Mod*). The H^+ efflux or Na^+ influx through NHE (J_{NHE}) is given by the equation

$$J_{NHE}(\text{mM/ms}) = N \times Mod\left([H^+]_i, [H^+]_o\right) \times j_{exch}\left([H^+]_i, [H^+]_o, [Na^+]_i, [Na^+]_o\right)/(A\, vol_i), \quad (1)$$

where N is the total number of NHE molecules, A is the Avogadro number, and vol_i is the intracellular volume.

The ion-exchanging part (j_{exch})

A ping-pong-type model with $1H^+$:$1Na^+$ stoichiometry (23) can be described with a six- or eight-state model (Fig. 1, *A* or *B*) by assuming that H^+ and Na^+ either can or cannot bind simultaneously to the transporter (23). In the six-state model, the steady-state turnover rate, j_{exch}, is given as

$$j_{exch} = \frac{\dfrac{k_1^+\frac{[Na^+]_o}{K_{Na}^o}}{\left(1+\frac{[Na^+]_o}{K_{Na}^o}+\frac{[H^+]_o}{K_H^o}\right)}\dfrac{k_2^+\frac{[H^+]_i}{K_H^i}}{\left(1+\frac{[Na^+]_i}{K_{Na}^i}+\frac{[H^+]_i}{K_H^i}\right)} - \dfrac{k_1^-\frac{[Na^+]_i}{K_{Na}^i}}{\left(1+\frac{[Na^+]_i}{K_{Na}^i}+\frac{[H^+]_i}{K_H^i}\right)}\dfrac{k_2^-\frac{[H^+]_o}{K_H^o}}{\left(1+\frac{[Na^+]_o}{K_{Na}^o}+\frac{[H^+]_o}{K_H^o}\right)}}{\dfrac{k_1^+\frac{[Na^+]_o}{K_{Na}^o}}{\left(1+\frac{[Na^+]_o}{K_{Na}^o}+\frac{[H^+]_o}{K_H^o}\right)}+\dfrac{k_2^+\frac{[H^+]_i}{K_H^i}}{\left(1+\frac{[Na^+]_i}{K_{Na}^i}+\frac{[H^+]_i}{K_H^i}\right)}+\dfrac{k_1^-\frac{[Na^+]_i}{K_{Na}^i}}{\left(1+\frac{[Na^+]_i}{K_{Na}^i}+\frac{[H^+]_i}{K_H^i}\right)}+\dfrac{k_2^-\frac{[H^+]_o}{K_H^o}}{\left(1+\frac{[Na^+]_o}{K_{Na}^o}+\frac{[H^+]_o}{K_H^o}\right)}}. \quad (2)$$

In the eight-state model, it is given as

$$j_{exch} = \frac{\dfrac{k_1^+\frac{[Na^+]_o}{K_{Na}^o}}{\left(1+\frac{[Na^+]_o}{K_{Na}^o}\right)\left(1+\frac{[H^+]_o}{K_H^o}\right)}\dfrac{k_2^+\frac{[H^+]_i}{K_H^i}}{\left(1+\frac{[Na^+]_i}{K_{Na}^i}\right)\left(1+\frac{[H^+]_i}{K_H^i}\right)} - \dfrac{k_1^-\frac{[Na^+]_i}{K_{Na}^i}}{\left(1+\frac{[Na^+]_i}{K_{Na}^i}\right)\left(1+\frac{[H^+]_i}{K_H^i}\right)}\dfrac{k_2^-\frac{[H^+]_o}{K_H^o}}{\left(1+\frac{[Na^+]_o}{K_{Na}^o}\right)\left(1+\frac{[H^+]_o}{K_H^o}\right)}}{\dfrac{k_1^+\frac{[Na^+]_o}{K_{Na}^o}}{\left(1+\frac{[Na^+]_o}{K_{Na}^o}\right)\left(1+\frac{[H^+]_o}{K_H^o}\right)}+\dfrac{k_2^+\frac{[H^+]_i}{K_H^i}}{\left(1+\frac{[Na^+]_i}{K_{Na}^i}\right)\left(1+\frac{[H^+]_i}{K_H^i}\right)}+\dfrac{k_1^-\frac{[Na^+]_i}{K_{Na}^i}}{\left(1+\frac{[Na^+]_i}{K_{Na}^i}\right)\left(1+\frac{[H^+]_i}{K_H^i}\right)}+\dfrac{k_2^-\frac{[H^+]_o}{K_H^o}}{\left(1+\frac{[Na^+]_o}{K_{Na}^o}\right)\left(1+\frac{[H^+]_o}{K_H^o}\right)}}, \quad (3)$$

where k values are rate constants and the K values are dissociation constants for individual ions. It is assumed that the binding and release of ions are instantaneous, and K values are not affected by binding of Na^+ or H^+ in the eight-state model.

The proton-modifier part (*Mod*)

Distinct from the ion-exchanging mechanism, NHE has an intracellular H^+-binding step for its activation (15). Since the value of the Hill coefficient (n_H) is still a matter of debate (24,25), we tested n_H values from 1 to 4 in data fitting of a Hill equation:

$$Mod = \frac{1}{1+\dfrac{(K_i)^{n_H}}{\left([H^+]_i\right)^{n_H}}}. \quad (4)$$

The pH_i-J_{NHE} relationship shifted in the acidic pH_i direction with decreasing pH_o in cardiac myocytes (21,22,26) and other cell types (24,27). However, the mechanism of depression by the extracellular H^+ has not been determined experimentally. Two mechanisms were considered here. First, the parallel shift may simply result from a competitive interaction between extracellular H^+ and Na^+ in the ion-exchanging part (24). In this case, the *Mod* remains the same as described by Eq. 4. Secondly, the parallel shift might occur when the extracellular H^+ directly modulates the proton-modifier part (Fig. 1 *C*), as expressed by

$$Mod = \frac{1}{1+\left(1+\dfrac{\left([H^+]_o\right)^{m_H}}{(K_o)^{m_H}}\right)\dfrac{(K_i)^{n_H}}{\left([H^+]_i\right)^{n_H}}}. \quad (5)$$

Mod in the former scheme is designated as *Mod1* (Eq. 4) and the latter as *Mod2* (Eq. 5). The Hill coefficient for extracellular H^+ (m_H) was

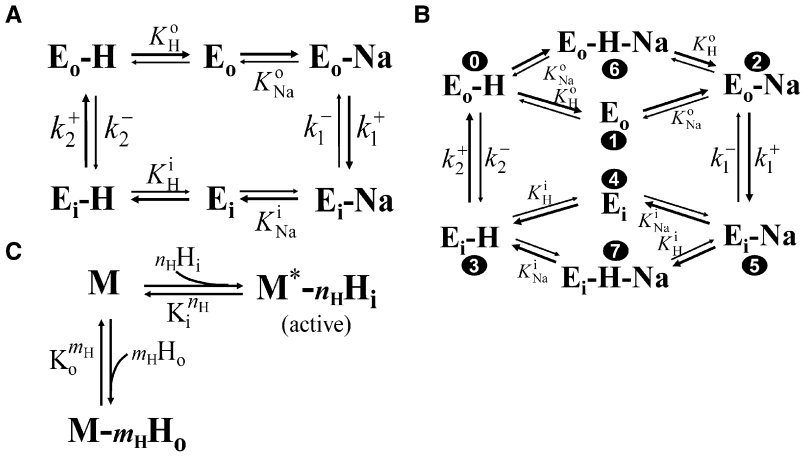

FIGURE 1 Schemes for the NHE model. Schemes for the ion-exchanging part: the six-state model (*A*) and the eight-state model (*B*). E_o represent the state in which the binding cavity opens to the outside of the cell and E_i is the state with the binding cavity open to the inside. The thick arrows indicate the forward direction. Definitions of the parameters are given in Table S1. The numerals in panel *B* indicate state labels that are referred to in Fig. 9 *B*. (*C*) Schemes for the proton-modifier part (M). Ion binding was assumed to be instantaneous with equilibrium constants, the *K* values. The asterisk indicates the state of M that activates E.

assumed to be 1 in this study, based on the experimental finding of $m_H = 1.2$ (21).

When the experimental data were fitted with Eq. 1, j_{exch} of a six- (Eq. 2) or eight-state (Eq. 3) model and *Mod1* (Eq. 4) or *Mod2* (Eq. 5) were examined. Since n_H ranged from 1 to 4, we examined 16 combinations of j_{exch} and *Mod* by data fitting.

Determination of unknown parameters

The ion-exchanging part of the NHE model was expressed as a closed-loop and constrained by the following microscopic reversibility (Eq. 6), leaving nine or 10 unknown parameters to be determined (see Table S1 in the Supporting Material):

$$\frac{K_H^i K_{Na}^o}{K_H^o K_{Na}^i} = \frac{k_1^+ k_2^+}{k_1^- k_2^-}. \quad (6)$$

Methods of fitting

The Levenberg-Marquardt fitting method was used to search for a minimum of chi-square (χ^2),

$$\chi^2 = \sum_{m=1}^{M} \left(\frac{y_m - y(x_m)}{\sigma_m} \right)^2, \quad (7)$$

where M is size of data set, y_m is experimental data of J_{NHE}, $y(x_m) = J_{NHE}([H^+]_i, [H^+]_o, [Na^+]_i$, or $[Na^+]_o)$ defined by Eq. 1 and σ_m is standard deviation (SD) for the m^{th} data point. We found that the χ^2 function of J_{NHE} had numerous local minimums in 9- or 10-dimensional parameter space. Therefore, local minimums were searched with initial values which were varied systematically within a physiological range (see Table S1), and then the least χ^2 was selected among them. The interval for varying initial values should be small enough to avoid missing the global minimum of the χ^2 function. As a compromise with computational cost, 3,674,160 starting points were used in each model scheme. Further consideration of the fitting method was presented in the Supporting Material.

Experimental data for determining model parameters

Selection of relevant experimental data is critical for constructing a precise model. We used three kinds of experimental data: the amplitude of J_{NHE} at various combinations of ($[H^+]_i$, $[H^+]_o$, $[Na^+]_i$, or $[Na^+]_o$), forward/reverse mode of ionic exchange, and the NHE turnover rate.

The measurements of NHE vary due to recording techniques (ion selective electrode or fluorescent dye) or differences in specimens (species (2), and muscles or isolated cells (28)). To minimize the experimental variations, systematic data were collected in sheep Purkinje fibers from two articles published by the same group (21,22) in which their established experimental methods were used. Alternatively, the experimental data from single ventricular myocytes might be adopted. As far as we compared, however, the configuration of pH_i-, pH_o-, and $[Na^+]_o$-J_{NHE} relationships obtained in dissociated ventricular myocyte were largely comparable to those in Purkinje fiber (see the Supporting Material). Furthermore, no measurement of $[Na^+]_i$-J_{NHE} relationship was available in ventricular myocytes. Therefore, we considered that the use of Purkinje fiber data was appropriate.

Despite the identical experimental methods in Purkinje fibers, NHE flux was still quite variable among different preparations. To fit the data set simultaneously, the amplitude of J_{NHE} was normalized with reference to common pH_i, pH_o, $[Na^+]_i$, and $[Na^+]_o$ in individual results. We assumed that the major subtype was NHE1 in Purkinje fibers (29) and that the diversity of NHE flux was mainly due to different sizes of tissue preparations. Finally, the data set of ion dependencies consisted of 106 data points ($M = 106$ in Eq. 7), shown in Fig. 3 *A* and Fig. 4, *A* and *B*, which include a few invisible points. To calculate χ^2, all variables in Eq. 1 and SD were

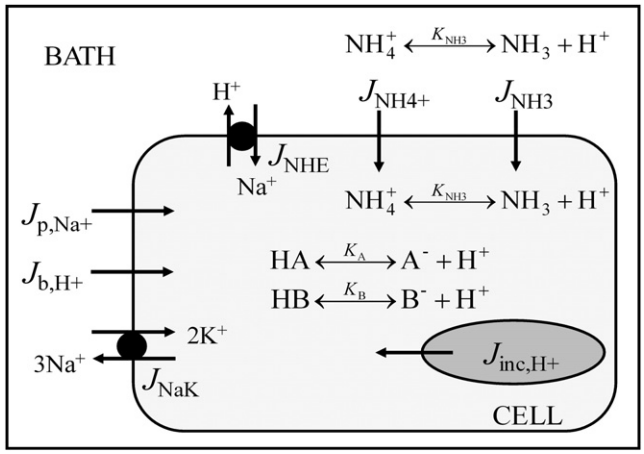

FIGURE 2 Simple cell model of cardiac Purkinje fibers. Abbreviations: $J_{p,Na+}$, passive flux of Na^+; $J_{b,H+}$, background H^+ flux; J_{NHE}, H^+ efflux or Na^+ influx through NHE; J_{NaK}, Na^+ efflux through the Na^+/K^+ pump; J_{NH3} and J_{NH4+}, passive fluxes of NH_3 and NH_4^+; and $J_{inc,H+}$, extra flux for intracellular H^+ increase by an unknown mechanism, which appears in Fig. 7. A^-, B^-, HA, and HB, free or H^+-bounded forms of intrinsic buffer species, A and B.

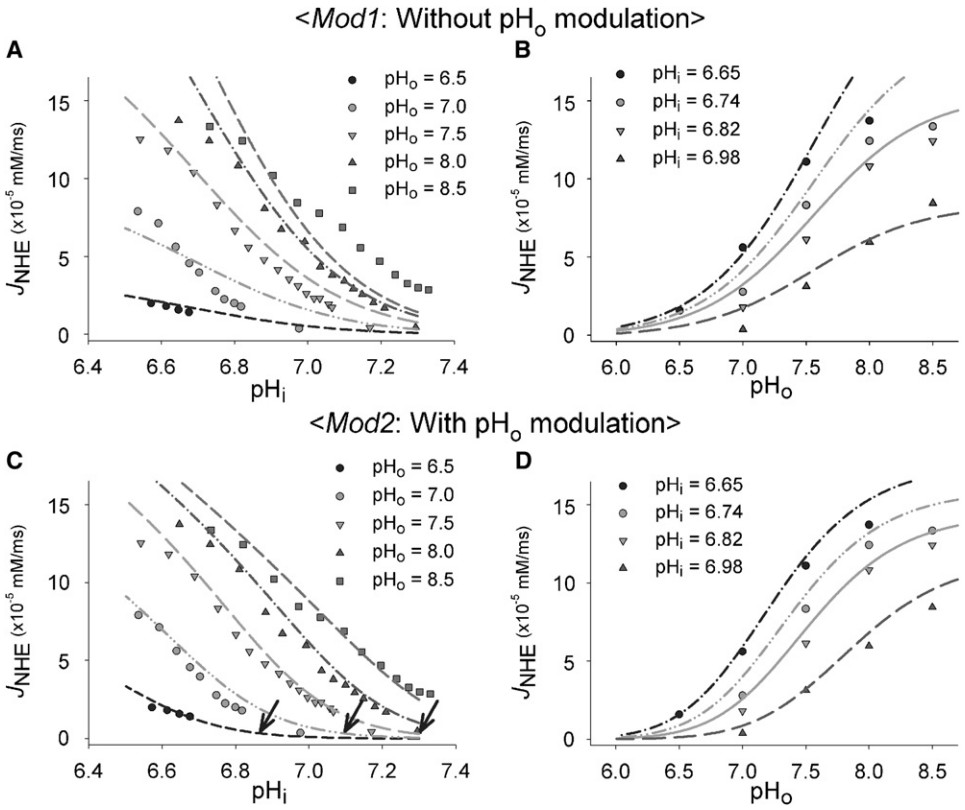

FIGURE 3 Comparison between *Mod1* and *Mod2* in response to pH_o variation. Experimental data (*symbols*) were taken from Vaughan-Jones and Wu (21). Various curves were plotted with the best fitting results for *Mod1* (*A* and *B*) or *Mod2* (*C* and *D*). Data points in panels *B* or *D* were selected from those in panels *A* or *C* for corresponding pH_i and pH_o, respectively. The arrows in panel *C* were fitted by eye to denote the location of each activation foot in the pH_i-NHE relationship at $pH_o = 6.5$, 7.0, and 7.5, respectively. Although data points were fitted with different $[Na^+]_i$, an average $[Na^+]_i$ was used to draw a continuous curve. This approximation may be justified, as the $[Na^+]_i$-J_{NHE} relation is shallow.

required, but $[Na^+]_i$ or SD was not always given in the literature. Therefore, $[Na^+]_i$ was supplemented from preliminary whole-cell simulations, and the ratio between SD and the mean of J_{NHE} described in the literature (25,30) was used for obtaining SD.

The forward/reverse mode of exchange was investigated in NHE1-transfected cells by measuring $^{22}Na^+$ flux (15). The forward mode offered information about the saturation of NHE activity at acidic pH_i below 5.2. The reverse mode provided important evidence that NHE includes a proton-

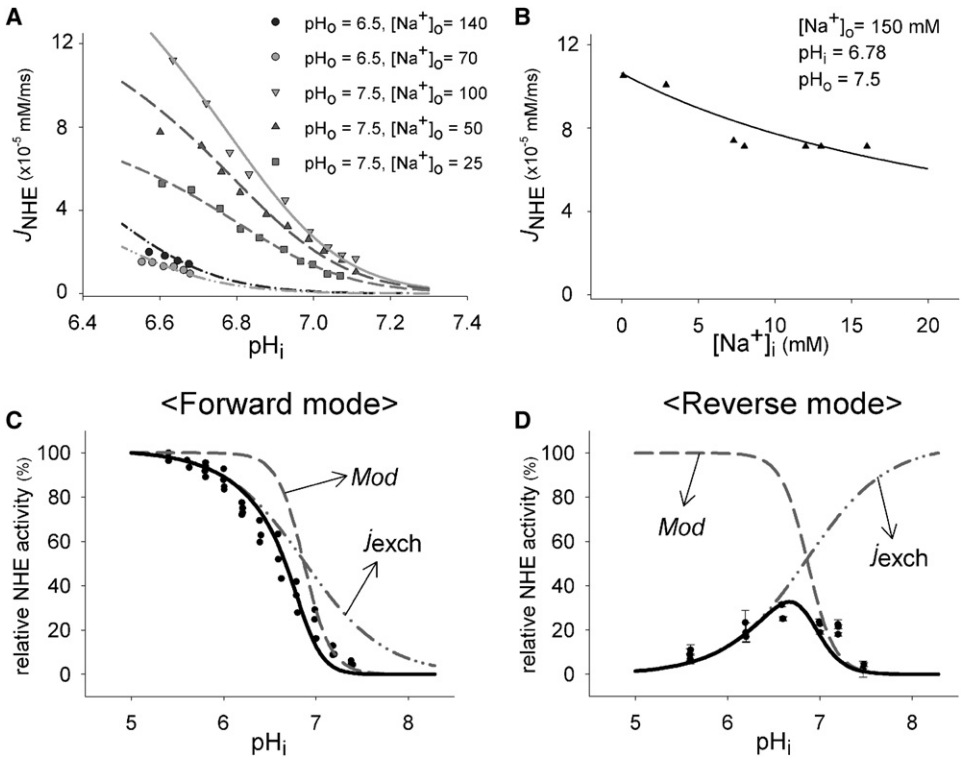

FIGURE 4 Best-fit results for NHE activity with *Mod2*. The data points in panels *A* and *B* (*symbols*) were taken from Wu and Vaughan-Jones (22). (*A*) pH_i-NHE relationship at various $[Na^+]_o$ and pH_o. As with Fig. 3, an average $[Na^+]_i$ was used to draw a continuous curve. (*B*) $[Na^+]_i$-NHE relationship. (*C* and *D*) The activities in the forward/reverse mode were simulated for $[Na^+]_i$ /$[Na^+]_o = 0$ / 1 or 1 / 0 mM, based on the experimental studies (15). The J_{NHE} curves (*bold lines*) were determined from the product of j_{exch} and *Mod* (Eq. 1).

modifier part in addition to ion-exchanging part, and helped us to determine j_{exch} and *Mod* separately. The turnover rate was measured by dividing J_{NHE} by total number of NHE molecules in experiments (31,32), which correspond to (*Mod* × j_{exch}) in Eq. 1. The turnover rate of one NHE1 molecule is 2–10 ms^{-1} at $pH_i = 6.0$, $pH_o = 7.4$, $[Na^+]_i$ ~0, and $[Na^+]_o = 140$ mM. We restricted this value to 2.3–2.5 ms^{-1} to avoid redundancies in the fitting results due to the inverse relationship between *N* and *k* values (refer to Eqs. 1–3).

Construction of a simple cell model

When pH_i recovers from acidification, $[Na^+]_i$ concurrently increases due to Na^+ influx through NHE. To check whether the experimental increase of $[Na^+]_i$ during pH_i recovery is attributable to the NHE activity, we incorporated the new NHE model into a simple cell model including the minimum components involved in pH_i or $[Na^+]_i$ regulation (Fig. 2). NBC and Cl^--HCO_3^- exchange were not considered because they are almost inactive in a HEPES-buffered system (1). A contribution of Cl^--OH^- exchange was included in a passive H^+ flux.

The equations for individual components are presented in the Appendix. For intracellular pH buffer (Eqs. 22–25), two intrinsic buffering species, A and B, were assumed. The total concentration and dissociation constants of A and B were determined based on the measurement of intrinsic pH buffering power in Purkinje fibers (33) (see the Supporting Material). Passive Na^+ flux (Eq. 13) is expressed by a constant field equation. The pH_i drift in Fig. 5 and Fig. 6 *B* in the absence of external Na^+ might be attributed to a background H^+. This flux seems to be larger at lower pH_o or at higher pH_i, and reversed to efflux at excessive acidic pH_i (22). Although Cl^--OH^- exchange is the potential candidate for the background H^+ flux in the CO_2/HCO_3^- free conditions (34,35), other unknown mechanisms might participate. Equation 14 is used only to describe the pH_i drift of unknown nature to complete the model fitting, but is not related to biophysical mechanisms. The equation for the Na^+/K^+ pump (Eq. 15) was adopted from the Kyoto model (36). We described flux of NH_4^+ with the constant field equation (Eq. 16) under the assumption that NH_4^+ is mainly transported through inwardly rectifying K^+ channels in cardiac myocytes (37). The NH_4^+ flux through Na^+/K^+ pump (38) or NHE (12) is neglected here, because the speed of acidification during NH_4Cl pulse is almost identical irrespective of the existence of Na^+ ion in intra-/extracellular medium (Fig. 5), which might affect NH_4^+ transport through Na^+/K^+ pump or NHE. Flux of NH_3 (Eq. 17) was expressed with Fick's law. The $[K^+]_i$ was set to be constant, assuming that K^+ permeability was dominant over others. For the same reason, the membrane potential was fixed at the K^+ equilibrium potential. This approximation is justified, since changes in the flux of Na^+ or NH_4^+ were small when the membrane potential was altered by $< \pm 10$ mV around the resting potential. The extracellular ionic composition was the same as that used in the experimental studies.

RESULTS

Determination of the NHE model scheme and parameters

The least χ^2 for the 16 model schemes were compared for different n_H values (see Table S2). Relatively large values were obtained with $n_H = 1$ for both *Mod1* and *Mod2*. However, it was difficult to determine which among $n_H = 2$, 3, and 4 was appropriate because of the marginal differences in χ^2. For the same reason, the six- and eight-state models of j_{exch} could not be differentiated.

A more careful approach than simple comparison of χ^2 was required to discriminate *Mod1* and *Mod2* because these

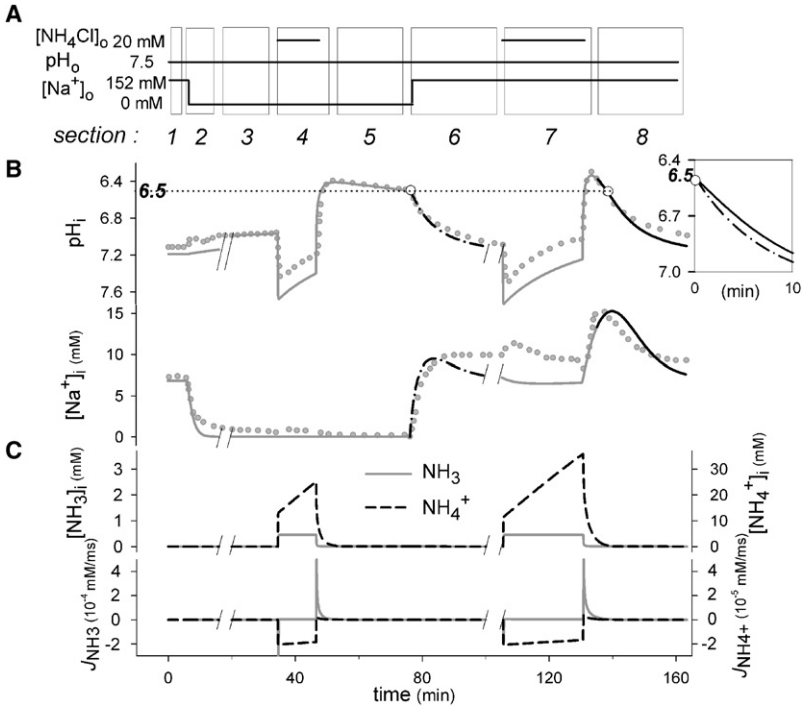

FIGURE 5 Simulation of pH_i and $[Na^+]_i$ variations in an NH_4Cl prepulse experiment. The original experimental recordings were from Fig. 5 in Wu and Vaughan-Jones (22). (*A*) The experimental protocol. (*B*) Changes of pH_i and $[Na^+]_i$ in the experiment (*shaded dots*) and in simulation (*lines*). (*Inset*) Comparison of the two recovery speeds at pH_i 6.5 between sections 6 and 8 in the simulation. Open circles indicate the time of comparison, which is indicated by a horizontal dotted line. The slash (//) denotes interruption of the simulation. (*C*) Simulated changes of $[NH_3]_i$, $[NH_4^+]_i$, J_{NH3}, and J_{NH4+}. ***Simulation of the response to an NH_4Cl prepulse***: The initial alkaline shift of pH_i was due to the almost instantaneous redistribution of NH_3 and the following relaxation is attributable to delayed accumulation of NH_4^+ within the cell. The subsequent sudden drop to pH_i 6.5 after removal of NH_4Cl was driven by the immediate and large efflux of NH_3. ***Determination of parameters for the cell model***: Cellular parameters were uniquely determined from the appropriate sections. $J_{b,H+}$ (Eq. 14) was determined from the slope of the pH change in sections 3 and 5, in which the other components were inactive due to the absence of Na^+. The amplitude of J_{NHE} (*N*) was determined by the recovery rate of pH_i in sections 8, where variation of $[Na^+]_i$ above 8 mM has little effect on NHE activity (22). J_{NaK} (*D* in Eq. 15) and $J_{p,Na+}$ (P_{Na+} in Eq. 13) were evaluated from the variations of $[Na^+]_i$ in sections 1 and 2. The parameters of J_{NH3} and J_{NH4+} (P_{NH3}, P_{NH4+} in Eqs. 16 and 17) were derived from section 4. P_{NH3} was determined by fitting the initial rising and final falling phase of pH_i record during NH_4Cl pulse, and P_{NH4+} from the slow acidification during the pulse and the rebound at the end of the pulse. P_{NH3} and P_{NH4+} had values comparable to those in previous simulation studies (46,47), if converted with a usual surface/volume ratio (36). The acid dissociation constant of NH_3/NH_4^+ (K_{NH3}) is 7.08×10^{-7} mM. We failed to avoid the small deviation of pH_i during NH_4Cl pulse when this common K_{NH3} was used for intracellular and extracellular medium. The values of model components are given in Table S3.

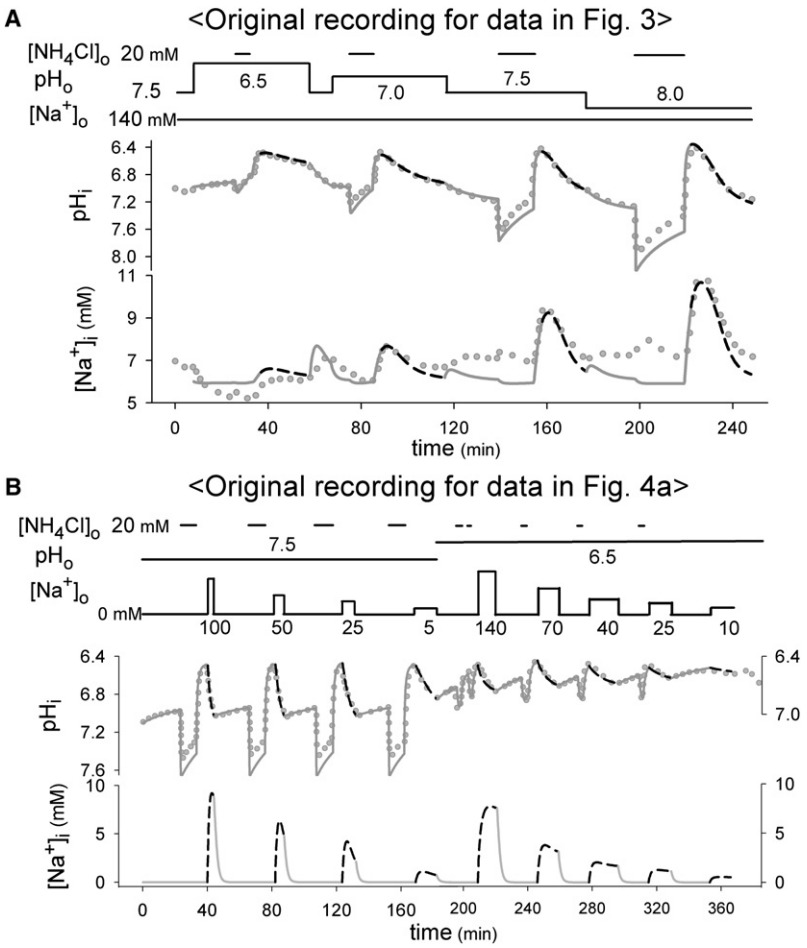

FIGURE 6 Simulations in various pH_o and $[Na^+]_o$. The experimental points (*shaded dots*) in panel *A* are from Fig. 6 in Vaughan-Jones and Wu (21) and those in panel *B* are from Fig. 1 in Wu and Vaughan-Jones (22). Dashed lines are simulated changes of pH_i and $[Na^+]_i$ in recovery periods from acidification. The values of model parameters were determined in a similar way to that in Fig. 5, except that *N* was already determined in the fitting procedure. In panel *B*, the parameters for J_{NaK} and $J_{p,Na+}$ determined in Fig. 5 were used, since $[Na^+]_i$ was not recorded in the original experiment. The values of model components are given in Table S3.

models had different numbers of unknown parameters. We found that the two models behaved differently in pH_o-induced inhibition (Fig. 3). *Mod2* could reconstruct the parallel shift of the pH_i-J_{NHE} relationship; that is, the activation foot moved to lower pH_i with decreasing pH_o (*arrows* in Fig. 3 *C*). Moreover, the pH_o-J_{NHE} relationship showed a clear saturation with increasing pH_o in agreement with experimental data (Fig. 3 *D*). In contrast, all the best-fit schemes of *Mod1* showed only scaling down in the NHE activity and failed to reconstruct the parallel shift of the pH_i-J_{NHE} and saturation by pH_o (Fig. 3, *A* and *B*). Therefore, we chose *Mod2* for characterizing the modulation by pH_o, which is in accord with the extracellular allosteric regulation suggested by Vaughan-Jones and Wu (21) and Vaughan-Jones and Spitzer (39).

Among the six plausible schemes for *Mod2*, we adopted the model using $n_H = 3$ with the eight-state ion-exchanging for the following simulations, simply because this model had the least χ^2, regardless of whether the difference between this and the other models was significant. The final parameter set (presented in Table S1) successfully reconstructed the dependencies on pH_i, $[Na^+]_o$, and $[Na^+]_i$ (Fig. 4, *A* and *B*), as well as the forward/reverse mode of NHE (Fig. 4, *C* and *D*) (15). We found that in the forward mode, the activation foot is determined by *Mod*, whereas the saturation at lower pH_i is dependent on j_{exch}. The slope is largely determined by cooperative activation in *Mod* with $n_H = 3$. In the reverse mode, j_{exch} and *Mod* change in opposite directions and J_{NHE} becomes bell-shaped.

Reconstruction of variations of pH_i and $[Na^+]_i$ in experimental recordings

Increase in $[Na^+]_i$ in NH_4Cl prepulse experiments

Wu and Vaughan-Jones (22) elaborated the experimental protocol shown in Fig. 5 *A* to examine effects of varying $[Na^+]_i$ on J_{NHE}. As the cell recovered from acidification in sections 6 and 8 in simulation (as depicted in Fig. 5), the counter Na^+ influx through NHE increased $[Na^+]_i$ to levels comparable to those in the experiment (Fig. 5 *B*). In both experiment and simulation, the range of $[Na^+]_i$ variation in section 6 was lower than that in section 8, and the initial rate of pH_i recovery was faster in section 6 (*inset* in Fig. 5). Since the simulation revealed that NH_3 and NH_4^+ were completely washed-out at $pH_i = 6.5$ (Fig. 5 *C*), it excluded the possibility that the remaining acid loading might retard recovery (an error factor mentioned in (21)). Thus, the

simulation results support the conclusion of Wu and Vaughan-Jones (22) that the different recovery speeds were caused by the depressed NHE activity at higher $[Na^+]_i$. For parameters of the cell model as well as mechanisms of inducing acidification by the NH_4Cl pulse, see Fig. 5 legend.

It is essential to consider variations of $[Na^+]_i$ as well as pH_i in evaluating the magnitude of J_{NHE}. We simulated the original recordings for obtaining the data points in Fig. 3 and Fig. 4 *A*, in which pH_o and $[Na^+]_o$ were varied. In the experiment (Fig. 6 *A*) giving the data points in Fig. 3, the recording protocol was analogous to section 8 in Fig. 5 and $[Na^+]_i$ varied over the range from 6 to 10 mM in both experiment and simulation. From the $[Na^+]_i$-J_{NHE} relationship (Fig. 4 *B*), it is evident that the magnitude of J_{NHE} in Fig. 3 is hardly affected by variations of $[Na^+]_i$ above 6 mM. On the other hand, the experimental protocol for the data points in Fig. 4 *A* (Fig. 6 *B*) is similar to that in section 6 in Fig. 5, and $[Na^+]_i$ increased from virtually 0 to various peak levels during recovery from acidification. Therefore, the amplitude of J_{NHE} in Fig. 4 *A* was clearly modified by the $[Na^+]_i$ variation, and that was why we supplemented individual experimental points in Fig. 4 *A* with corresponding values of $[Na^+]_i$ obtained by simulations (mentioned as preliminary simulations in Methods). Taken together, these simulation results confirmed that our NHE model is applicable when extracellular conditions are changed.

Acidification induced indirectly by blocking the Na^+/K^+ pump

An increase in $[Na^+]_i$ has been suggested to mediate the intracellular acidification when the Na^+/K^+ pump is inhibited through two mechanisms:

1. A depression of NHE activity due to a decrease in the transmembrane Na^+ gradient (40).
2. An induction of intracellular acidification linked to an increase of $[Ca^{2+}]_i$ through depression of Na^+-Ca^{2+} exchanger (NCX) (41,42).

First, we examined the extent of acidification induced by attenuating J_{NHE} through increased $[Na^+]_i$ (*black line* in Fig. 7). When 50% of the Na^+/K^+ pump was inhibited by 10 μM strophanthidin ($K_D = 1.12 \times 10^{-5}$ M (43)), $[Na^+]_i$ rose rapidly toward a saturating level beyond 16 mM, in agreement with the experimental data. However, pH_i was only reduced by 0.05, which was much smaller than the experimental drop of ~0.3. Next, we tested the second mechanism, in which an extra H^+ increment ($j_{inc,H+}$) occurs through an increase in $[Ca^{2+}]_i$ (*red line* in Fig. 7) (41). If $[Ca^{2+}]_i$ is mainly equilibrated by NCX in cardiac myocytes, $[Ca^{2+}]_i$ is a function of $[Na^+]_i^3$, provided that $[Ca^{2+}]_o$ and $[Na^+]_o$ remain constant:

$$\frac{[Ca^+]_i}{[Ca^+]_o} = \left(\frac{[Na^+]_i}{[Na^+]_o}\right)^3 \exp\left(\frac{V_m F}{RT}\right) \quad (8)$$

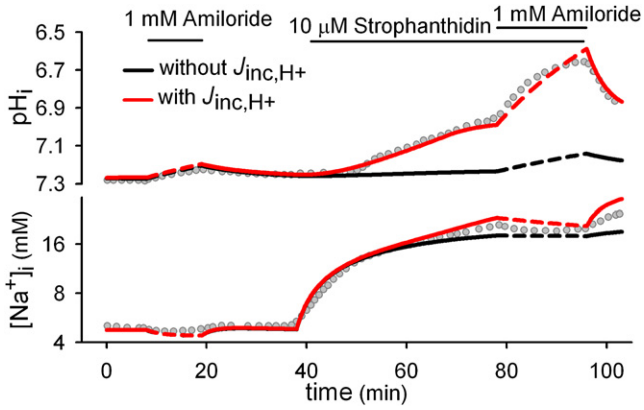

FIGURE 7 Effects of blocking the Na^+/K^+ pump on pH_i and $[Na^+]_i$. The original experimental recordings (*gray dots*) are taken from Fig. 2 in Kaila and Vaughan-Jones (42). Simulation results with (*red lines*) or without (*black lines*) an extra H^+ increment ($J_{inc,H+}$) are shown. Dashed lines indicate changes induced by applying amiloride. Most parameter values are the same as in Fig. 5, since the experimental conditions were comparable. The amplitudes of $J_{b,H+}$ and J_{NHE} were slightly modified to adjust the steady-state values of pH_i and $[Na^+]_i$ at time zero. The values of model components are given in Table S3.

(see Blaustein and Leder (44)). For simplicity, we assumed that $j_{inc,H+}$ is linearly proportional to $[Ca^{2+}]_i$ (or $[Na^+]_i^3$) within a limit (Eq. 18). In consequence, a decline of pH_i with an obvious delayed onset was obtained as in the experiment (see also (40)). In addition, the simulation successfully reconstructed the increased rate of acidification and the decrease of $[Na^+]_i$ during the complete blockage of NHE in the presence of strophanthidin in comparison to the control run. Although Eq. 18 is only a phenomenological description, the simulation supports the view that a Ca^{2+}-induced H^+ increment from an unknown origin contributes to acidification to a larger extent than depression of J_{NHE} through an increase in $[Na^+]_i$.

DISCUSSION

Here, for the first time to our knowledge, we have reconstructed the transient increase in $[Na^+]_i$ accompanying NHE activation at different $[Na^+]_o$ and pH_o. So far, there are two articles that offered simulated effects of acidosis on the developed tension with a cell model including electrical excitation, Ca^{2+} dynamics by the sarcoplasmic reticulum, contraction, and the modulation of various molecular functions at acidic pH_i (9,13). In contrast to those complicated simulations, we focused our simulations totally on the Purkinje fiber experiments, which recorded the time course of $[Na^+]_i$ variation caused by the NHE activation. For deeper understanding of regulation of $[Na^+]_i$ at different pH_i, we will discuss functional coupling between NHE and Na^+/K^+ pump during acidosis. We then determine the extent of $[Na^+]_i$ increase induced by acidosis using steady-state pH_i-$[Na^+]_i$ relationship, and discuss $[Na^+]_i$-J_{NHE} relationship by taking the thermodynamic driving force into account.

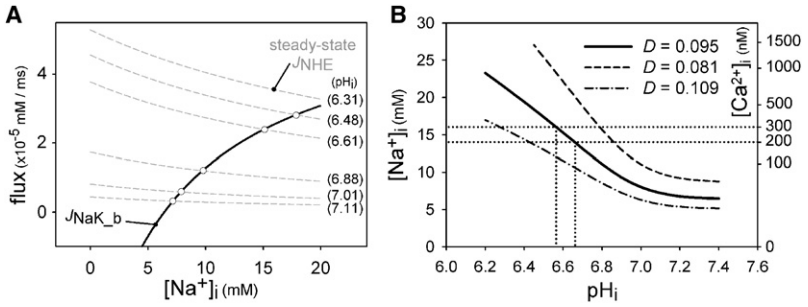

FIGURE 8 Steady-state relationship between pH_i and $[Na^+]_i$. (*A*) Na^+ flux balance between J_{NHE} and J_{NaK_b}. Gray curves indicate $[Na^+]_i$-J_{NHE} at the different pH_i values indicated on the right, and the black curve indicates J_{NaK_b}. Intersections of the J_{NHE} with J_{NaK_b} are marked with open circles. (*B*) The steady-state relationship between pH_i and $[Na^+]_i$, corresponding to intersections of the J_{NHE} and J_{NaK_b} in panel *A*. When the amplitude of the Na^+/K^+ pump was altered from $D = 0.095$ to $D = 0.081$ or 0.109, the curve shifted as indicated by the dashed lines. The steady-state $[Na^+]_i$ on the left axis was converted to $[Ca^{2+}]_i$ on the right axis using Eq. 8. The dotted lines indicate the critical levels of $[Na^+]_i$ and pH_i. The calculations were all conducted under the condition of a membrane potential of −52 mV, a reversal potential of K^+ at 20 mM $[K^+]_o$.

Relationship between acidosis and $[Na^+]_i$ or $[Ca^{2+}]_i$

The variation of $[Na^+]_i$ is determined by the balance among NHE, Na^+/K^+ pump, and passive Na^+ flux in our simple cell model. The time derivative of $[Na^+]_i$ is

$$\frac{d[Na^+]_i}{dt} = J_{NHE} - (J_{NaK} + J_{p,Na+})$$

(see Eq. 19). Since $[K^+]_o$ and the membrane potential are assumed to be constant, both J_{NaK} and $J_{p,Na+}$ are functions of only $[Na^+]_i$. To examine the major interaction between NHE and Na^+/K^+ pump, the sum of J_{NaK} and $J_{p,Na+}$ is treated as J_{NaK_b}, which is J_{NaK} biased by $J_{p,Na+}$ (Fig. 8 *A*). The intersections of the J_{NaK_b} and J_{NHE} curves correspond to $d[Na^+]_i/dt = 0$ and give steady-state values of $[Na^+]_i$ at each pH_i. This steady-state relationship is demonstrated by the continuous curve in Fig. 8 *B*. $[Na^+]_i$ is nearly constant on the alkaline side above pH_i 7.2 and increases linearly with acidosis. This Na^+ overload during persistent acidosis may affect cellular viability via a secondary $[Ca^{2+}]_i$ increment through NCX (45), which causes myocardial contracture. To investigate the critical level of acidosis, $[Na^+]_i$ is converted to $[Ca^{2+}]_i$ according to Eq. 8 (*right axis* in Fig. 8 *B*). Assuming that blood pumping of the ventricle is interfered with when diastolic $[Ca^{2+}]_i$ remains higher than the activation threshold of contraction at 200 or 300 nM, the critical $[Na^+]_i$ is 14–16 mM, or the critical pH_i is ~6.6. The critical pH_i moves in the acidic direction when J_{NaK} is depressed, and in the alkaline direction with enhanced J_{NaK} (*dotted lines* in Fig. 8 *B*). Similarly, the change in membrane leak conductance ($J_{p,Na+}$ in our model) under pathophysiological conditions may also affect the critical level of pH_i. To get a deeper insight into the critical level of acidosis, note that the pH sensitivity of channels, transporters, and contraction should also be accounted for in the model calculation in future.

Relationship between thermodynamic driving force and J_{NHE}

The variation of $[Na^+]_i$ affects the J_{NHE} via thermodynamic driving force, E_d, which is given as

$$E_d = RT \times \left(\ln\frac{[H^+]_i}{[H^+]_o} + \ln\frac{[Na^+]_o}{[Na^+]_i} \right). \quad (9)$$

With a constant pH_o/pH_i gradient and a fixed $[Na^+]_o$, E_d is a linear function of $\ln([Na^+]_i)$ and reverses its sign at an equilibrium value of $[Na^+]_i$ (Fig. 9 *A*). It should be noted that our model successfully defines the equilibrium value of $[Na^+]_i$ by adopting microscopic reversibility. Fig. 9 *A* indicates that the magnitude of J_{NHE} saturates below 3 mM $[Na^+]_i$ despite the linear increase of E_d. The dependency of J_{NHE} on E_d is given by the following equation, in analogy to Ohm's law,

$$J_{NHE} = gE_d, \quad (10)$$

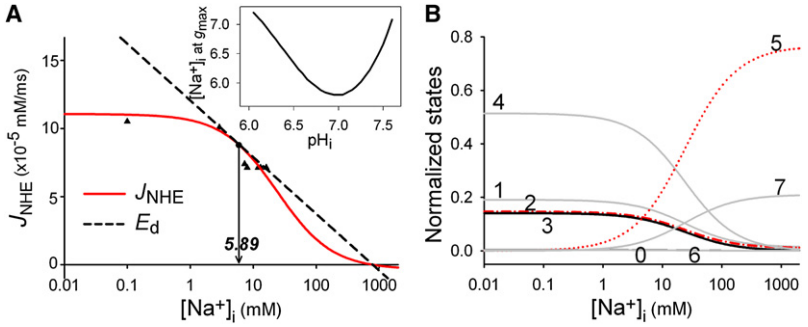

FIGURE 9 Variation of J_{NHE} and E_d, and transition of model states with $[Na^+]_i$. (*A*) The $[Na^+]_i$-J_{NHE} relationship (*solid line*) and E_d (*dashed line*) with a log scale for $[Na^+]_i$. J_{NHE} and data points (*triangles*) are identical, as shown in Fig. 4 *B*. E_d is zero at $[Na^+]_i = 787$ mM at $pH_i = 6.78$, $pH_o = 7.5$, and $[Na^+]_o = 150$ mM. (*Inset*) Point of tangency for g_{max} at each pH_i. (*B*) Distribution of states for the ion-exchanging part as a function of $[Na^+]_i$. Numerals indicate the states of NHE model, as defined in Fig. 1 *B*.

where g is the conductance of NHE (mol J^{-1} ms^{-1}) and is defined by the slope connecting each point on the J_{NHE} curve with the equilibrium point. The maximum g, g_{max}, appeared at $[Na^+]_i = 5.89$ mM, which is defined by a tangent line to the J_{NHE} at $pH_i = 6.78$. The values of $[Na^+]_i$ giving g_{max} were explored at various pH_i and are plotted against pH_i (*inset* of Fig. 9). It is evident that $[Na^+]_i$ at g_{max} remains in a narrow range over a wide range of pH_i; that is, the NHE model operates almost at g_{max} over the physiological range of $[Na^+]_i$, even during severe acidosis.

The $[Na^+]_i$ dependency of J_{NHE} or g is determined by the state distributions of the ion-exchanging part of the NHE model, as shown in Fig. 9 *B*:

$$J_{NHE} \propto (\text{state } 2)k_1^+ - (\text{state } 5)k_1^-. \tag{11}$$

When intracellular Na^+ is depleted, state 5, in which Na^+ binds on the intracellular side, becomes nearly 0. Accordingly, J_{NHE} is only dependent on state 2, thereby causing J_{NHE} to saturate. As $[Na^+]_i$ increases, states 5 and 7 accumulate at the expense of all the other states. An integrated effect of the variations of states 2 and 5 induces a gradual decay of g with increasing $[Na^+]_i$. Thus, the state rearrangement produces the sigmoidal dependency of J_{NHE} on $[Na^+]_i$ (Fig. 9 *A*).

APPENDIX

Equations for the simple cell model

$$CF_X = \frac{z_X F V_m}{RT} \frac{[X]_i - [X]_o \exp(-z_X F V_m/RT)}{1 - \exp(-z_X F V_m/RT)}, \text{ where } X = \{Na^+, NH_4^+\}. \tag{12}$$

$$J_{p,Na+} = P_{Na+} CF_{Na+}. \tag{13}$$

$$J_{b,H+} = A[H^+]_o + B\,pH_i + C. \tag{14}$$

$$J_{NaK} = D \frac{3 \times I_{NaK(\text{in kyoto model})}}{F\,vol_i}. \tag{15}$$

$$J_{NH4+} = P_{NH4+} CF_{NH4+}. \tag{16}$$

$$J_{NH3} = P_{NH3}([NH_3]_i - [NH_3]_o). \tag{17}$$

$$J_{inc,H+} = \begin{cases} E([Na^+]_i)^3 & (\text{when } J_{inc,H+} < Max_{inc,H+}) \\ Max_{inc,H+} & (\text{otherwise}) \end{cases}. \tag{18}$$

$$\frac{d[Na^+]_i}{dt} = J_{NHE} - J_{NaK} - J_{p,Na+}. \tag{19}$$

$$\frac{d([NH_3]_i + [NH_4^+]_i)}{dt} = -J_{NH3} - J_{NH4+}. \tag{20}$$

$$\frac{d([H^+]_i + [NH_4^+]_i + [HA]_i + [HB]_i)}{dt} = -J_{NHE} - J_{b,H+} - J_{NH4+} + J_{inc,H+}. \tag{21}$$

The following equilibrium reactions among NH_3, NH_4^+, H^+, and pH buffer A and B were calculated.

$$HA \overset{K_A}{\longleftrightarrow} A^- + H^+.$$

$$HB \overset{K_B}{\longleftrightarrow} B^- + H^+.$$

$$NH_4^+ \overset{K_{NH3}}{\longleftrightarrow} NH_3 + H^+.$$

$$[HA]_i + [A^-]_i = [TA]. \tag{22}$$

$$[HB]_i + [B^-]_i = [TB]. \tag{23}$$

$$K_A = \frac{[A^-]_i [H^+]_i}{[HA]_i}. \tag{24}$$

$$K_B = \frac{[B^-]_i [H^+]_i}{[HB]_i}. \tag{25}$$

$$K_{NH3} = \frac{[NH_3]_i [H^+]_i}{[NH_4^+]_i} = \frac{[NH_3]_o [H^+]_o}{[NH_4^+]_o}. \tag{26}$$

[TA] or [TB] is the total concentration of pH buffer of A or B, respectively. $[NH_3]_i$, $[NH_4^+]_i$, and $[H^+]_i$ were obtained by solving Eqs. 22–26 with the iteration method.

Definitions and values of the model parameters are given in Table S3.

SUPPORTING MATERIAL

One figure and three tables are available at http://www.biophysj.org/biophysj/supplemental/S0006-3495(09)01444-1.

The authors are grateful to Prof. T. Powell and colleagues in the Biosimulation projects of Kyoto University and Ritsumeikan University for continuous discussion during this study.

This work was supported by the Biomedical Cluster Kansai project of Ministry of Education, Culture, Sports, Science and Technology Japan.

REFERENCES

1. Leem, C. H., D. Lagadic-Gossmann, and R. D. Vaughan-Jones. 1999. Characterization of intracellular pH regulation in the guinea-pig ventricular myocyte. *J. Physiol.* 517:159–180.
2. Yamamoto, T., P. Swietach, A. Rossini, S. H. Loh, R. D. Vaughan-Jones, et al. 2005. Functional diversity of electrogenic Na^+-HCO_3^- cotransport in ventricular myocytes from rat, rabbit and guinea pig. *J. Physiol.* 562:455–475.
3. Vaughan-Jones, R. D., F. C. Villafuerte, P. Swietach, T. Yamamoto, A. Rossini, et al. 2006. pH-Regulated Na^+ influx into the mammalian ventricular myocyte: the relative role of Na^+-H^+ exchange and Na^+-HCO co-transport. *J. Cardiovasc. Electrophysiol.* 17 (Suppl 1):S134–S140.

4. ten Hove, M., J. G. van Emous, and C. J. van Echteld. 2003. Na^+ overload during ischemia and reperfusion in rat hearts: comparison of the Na^+/H^+ exchange blockers EIPA, cariporide and eniporide. *Mol. Cell. Biochem.* 250:47–54.
5. Hartmann, M., and U. K. Decking. 1999. Blocking Na^+-H^+ exchange by cariporide reduces Na^+-overload in ischemia and is cardioprotective. *J. Mol. Cell. Cardiol.* 31:1985–1995.
6. Kentish, J. C. 1999. A role for the sarcolemmal Na^+/H^+ exchanger in the slow force response to myocardial stretch. *Circ. Res.* 85:658–660.
7. Cingolani, H. E., N. G. Perez, E. A. Aiello, and M. C. de Hurtado. 2005. Intracellular signaling following myocardial stretch: an autocrine/paracrine loop. *Regul. Pept.* 128:211–220.
8. Crampin, E. J., N. P. Smith, A. E. Langham, R. H. Clayton, and C. H. Orchard. 2006. Acidosis in models of cardiac ventricular myocytes. *Philos. Transact. A Math. Phys. Eng. Sci.* 364:1171–1186.
9. Ch'en, F. F., R. D. Vaughan-Jones, K. Clarke, and D. Noble. 1998. Modeling myocardial ischemia and reperfusion. *Prog. Biophys. Mol. Biol.* 69:515–538.
10. Swietach, P., and R. D. Vaughan-Jones. 2005. Spatial regulation of intracellular pH in the ventricular myocyte. *Ann. N.Y. Acad. Sci.* 1047:271–282.
11. Alexander, R. T., A. Malevanets, A. M. Durkan, H. S. Kocinsky, P. S. Aronson, et al. 2007. Membrane curvature alters the activation kinetics of the epithelial Na^+/H^+ exchanger, NHE3. *J. Biol. Chem.* 282:7376–7384.
12. Weinstein, A. M. 1995. A kinetically defined Na^+/H^+ antiporter within a mathematical model of the rat proximal tubule. *J. Gen. Physiol.* 105:617–641.
13. Crampin, E. J., and N. P. Smith. 2006. A dynamic model of excitation-contraction coupling during acidosis in cardiac ventricular myocytes. *Biophys. J.* 90:3074–3090.
14. Niederer, S. A., and N. P. Smith. 2007. A mathematical model of the slow force response to stretch in rat ventricular myocytes. *Biophys. J.* 92:4030–4044.
15. Wakabayashi, S., T. Hisamitsu, T. Pang, and M. Shigekawa. 2003. Kinetic dissection of two distinct proton binding sites in Na^+/H^+ exchangers by measurement of reverse mode reaction. *J. Biol. Chem.* 278:43580–43585.
16. Moncoq, K., G. Kemp, X. Li, L. Fliegel, and H. S. Young. 2008. Dimeric structure of human Na^+/H^+ exchanger isoform 1 overproduced in *Saccharomyces cerevisiae*. *J. Biol. Chem.* 283:4145–4154.
17. Otsu, K., J. Kinsella, B. Sacktor, and J. P. Froehlich. 1989. Transient state kinetic evidence for an oligomer in the mechanism of Na^+-H^+ exchange. *Proc. Natl. Acad. Sci. USA.* 86:4818–4822.
18. Otsu, K., J. L. Kinsella, P. Heller, and J. P. Froehlich. 1993. Sodium dependence of the Na^+-H^+ exchanger in the pre-steady state. Implications for the exchange mechanism. *J. Biol. Chem.* 268:3184–3193.
19. Lacroix, J., M. Poet, C. Maehrel, and L. Counillon. 2004. A mechanism for the activation of the Na/H exchanger NHE-1 by cytoplasmic acidification and mitogens. *EMBO Rep.* 5:91–96.
20. Fuster, D., O. W. Moe, and D. W. Hilgemann. 2008. Steady-state function of the ubiquitous mammalian Na/H exchanger (NHE1) in relation to dimer coupling models with 2Na/2H stoichiometry. *J. Gen. Physiol.* 132:465–480.
21. Vaughan-Jones, R. D., and M. L. Wu. 1990. Extracellular H^+ inactivation of Na^+-H^+ exchange in the sheep cardiac Purkinje fiber. *J. Physiol.* 428:441–466.
22. Wu, M. L., and R. D. Vaughan-Jones. 1997. Interaction between Na^+ and H^+ ions on Na-H exchange in sheep cardiac Purkinje fibers. *J. Mol. Cell. Cardiol.* 29:1131–1140.
23. Aronson, P. S. 1985. Kinetic properties of the plasma membrane Na^+-H^+ exchanger. *Annu. Rev. Physiol.* 47:545–560.
24. Green, J., D. T. Yamaguchi, C. R. Kleeman, and S. Muallem. 1988. Cytosolic pH regulation in osteoblasts. Interaction of Na^+ and H^+ with the extracellular and intracellular faces of the Na^+/H^+ exchanger. *J. Gen. Physiol.* 92:239–261.
25. Wallert, M. A., and O. Frohlich. 1989. Na^+-H^+ exchange in isolated myocytes from adult rat heart. *Am. J. Physiol.* 257:C207–C213.
26. van Borren, M. M., A. Baartscheer, R. Wilders, and J. H. Ravesloot. 2004. NHE-1 and NBC during pseudo-ischemia/reperfusion in rabbit ventricular myocytes. *J. Mol. Cell. Cardiol.* 37:567–577.
27. Jean, T., C. Frelin, P. Vigne, P. Barbry, and M. Lazdunski. 1985. Biochemical properties of the Na^+/H^+ exchange system in rat brain synaptosomes. Interdependence of internal and external pH control of the exchange activity. *J. Biol. Chem.* 260:9678–9684.
28. Bountra, C., T. Powell, and R. D. Vaughan-Jones. 1990. Comparison of intracellular pH transients in single ventricular myocytes and isolated ventricular muscle of guinea-pig. *J. Physiol.* 424:343–365.
29. Petrecca, K., R. Atanasiu, S. Grinstein, J. Orlowski, and A. Shrier. 1999. Subcellular localization of the Na^+/H^+ exchanger NHE1 in rat myocardium. *Am. J. Physiol.* 276:H709–H717.
30. Hoffmann, G., Y. Ko, A. Sachinidis, B. O. Gobel, H. Vetter, et al. 1995. Kinetics of Na^+/H^+ exchange in vascular smooth muscle cells from WKY and SHR: effects of phorbol ester. *Am. J. Physiol.* 268:C14–C20.
31. Ng, L. L., J. E. Davies, M. Siczkowski, F. P. Sweeney, P. A. Quinn, et al. 1994. Abnormal Na^+/H^+ antiporter phenotype and turnover of immortalized lymphoblasts from type 1 diabetic patients with nephropathy. *J. Clin. Invest.* 93:2750–2757.
32. Siczkowski, M., J. E. Davies, and L. L. Ng. 1994. Activity and density of the Na^+/H^+ antiporter in normal and transformed human lymphocytes and fibroblasts. *Am. J. Physiol.* 267:C745–C752.
33. Vaughan-Jones, R. D., and M. L. Wu. 1990. pH dependence of intrinsic H^+ buffering power in the sheep cardiac Purkinje fiber. *J. Physiol.* 425:429–448.
34. Sun, B., C. H. Leem, and R. D. Vaughan-Jones. 1996. Novel chloride-dependent acid loader in the guinea-pig ventricular myocyte: part of a dual acid-loading mechanism. *J. Physiol.* 495:65–82.
35. Niederer, S. A., P. Swietach, D. A. Wilson, N. P. Smith, and R. D. Vaughan-Jones. 2008. Measuring and modeling chloride-hydroxyl exchange in the Guinea-pig ventricular myocyte. *Biophys. J.* 94:2385–2403.
36. Matsuoka, S., N. Sarai, S. Kuratomi, K. Ono, and A. Noma. 2003. Role of individual ionic current systems in ventricular cells hypothesized by a model study. *Jpn. J. Physiol.* 53:105–123.
37. Mitra, R. L., and M. Morad. 1991. Permeance of Cs^+ and Rb^+ through the inwardly rectifying K^+ channel in guinea pig ventricular myocytes. *J. Membr. Biol.* 122:33–42.
38. Bielen, F. V., H. G. Glitsch, and F. Verdonck. 1991. Dependence of Na^+ pump current on external monovalent cations and membrane potential in rabbit cardiac Purkinje cells. *J. Physiol.* 442:169–189.
39. Vaughan-Jones, R. D., and K. W. Spitzer. 2002. Role of bicarbonate in the regulation of intracellular pH in the mammalian ventricular myocyte. *Biochem. Cell Biol.* 80:579–596.
40. Deitmer, J. W., and D. Ellis. 1980. Interactions between the regulation of the intracellular pH and sodium activity of sheep cardiac Purkinje fibers. *J. Physiol.* 304:471–488.
41. Vaughan-Jones, R. D., W. J. Lederer, and D. A. Eisner. 1983. Ca^{2+} ions can affect intracellular pH in mammalian cardiac muscle. *Nature.* 301:522–524.
42. Kaila, K., and R. D. Vaughan-Jones. 1987. Influence of sodium-hydrogen exchange on intracellular pH, sodium and tension in sheep cardiac Purkinje fibers. *J. Physiol.* 390:93–118.
43. Levi, A. J. 1991. The effect of strophanthidin on action potential, calcium current and contraction in isolated guinea-pig ventricular myocytes. *J. Physiol.* 443:1–23.
44. Blaustein, M. P., and W. J. Lederer. 1999. Sodium/calcium exchange: its physiological implications. *Physiol. Rev.* 79:763–854.
45. Baartscheer, A. 2006. Chronic inhibition of Na^+/H^+-exchanger in the heart. *Curr. Vasc. Pharmacol.* 4:23–29.
46. Boron, W. F., and P. De Weer. 1976. Intracellular pH transients in squid giant axons caused by CO_2, NH_3, and metabolic inhibitors. *J. Gen. Physiol.* 67:91–112.
47. Benjelloun, F., N. Bakouh, J. Fritsch, P. Hulin, J. Lipecka, et al. 2005. Expression of the human erythroid Rh glycoprotein (RhAG) enhances both NH_3 and NH_4^+ transport in HeLa cells. *Pflugers Arch.* 450:155–167.